REPORT DOCUMENTATION PAGE

AFRL-SR-AR-TR-04-

0594

1. AGENCY USE ONLY *(Leave blank)*

2. REPORT DATE
10 NOV 04

3. REPORT TYPE AND DATES COVERED
FINAL REPORT 1 AUG 02 TO 31 JAN 04

4. TITLE AND SUBTITLE
DYNAMICS OF O(3P) REACTIONS WITH GASEOUS, LIQUID, AND SOLID HYDROCARBONS

5. FUNDING NUMBERS
F49620-02-1-0401

6. AUTHOR(S)
DR WILLIAM L. HASE

7. PERFORMING ORGANIZATION NAME(S) AND ADDRESS(ES)
WAYNE STATE UNIVERSITY
DEPARTMENT OF COMPUTER SCIENCE
5143 CASS AVE., ROOM 431 STATE HALL
DETROIT, MI 48202

8. PERFORMING ORGANIZATION REPORT NUMBER

9. SPONSORING/MONITORING AGENCY NAME(S) AND ADDRESS(ES)

AFOSR/NL
4015 WILSON BLVD., ROOM 713
ARLINGTON, VA 22203-1954

10. SPONSORING/MONITORING AGENCY REPORT NUMBER

11. SUPPLEMENTARY NOTES

12a. DISTRIBUTION AVAILABILITY STATEMENT

APPROVE FOR PUBLIC RELEASE: DISTRIBUTION UNLIMITED.

12b. DISTRIBUTION CODE

13. ABSTRACT *(Maximum 200 words)*

This final report describes the initial two phases of the overall project. In the first phase, accurate barriers and e4nergetics were calculated for 7 reactions involved in O(3P) oxidation of hydrocarbons. This was done by MRCI/CASSCF ab initio calculations with cc-pVTZ and cc-pVQZ basis sets and extrapolation to the complete basis set limit. For collisions of high-energy O(3P) atoms with hydrocarbons, the radical products contain sufficient internal energy to undergo unimolecular decomposition. Tests showed that PMP2//UMP2/cc-pVTZ gives accuratge energies and transition state properties for these reactions, and this information was also used to characterize the potential energy surface for hydrocarbon oxidation. In the second phase, the PM3 semiempirical quantum chemistry method, with a UHF wavefunction, was modified and parameterized with specific reaction parameters (SRPs) to fit the ab initio barriers, reactions energies, and geometries determined in phase 1. The resulting method, PM3-SRP, gives a good fit to the ab initio data. The PM3-SRP method was tested in a trajectory study of the O(3P) + C2H6 > OH + C2H5 reaction dynamics. The results agree with experiment.

14. SUBJECT TERMS

20041129 039

15. NUMBER OF PAGES

16. PRICE CODE

17. SECURITY CLASSIFICATION OF REPORT

18. SECURITY CLASSIFICATION OF THIS PAGE

19. SECURITY CLASSIFICATION OF ABSTRACT

20. LIMITATION OF ABSTRACT

AFOSR GRANT:	Dynamics of $O(^3P)$ Reactions with Gaseous, Liquid, and Solid Hydrocarbons
AFOSR PROGRAM MANAGER:	Michael Berman
CONTRACT NUMBER:	F49620-02-1-0401
PRINCIPAL INVESTIGATOR (PI):	William L. Hase
PI INSTITUTION:	Wayne State University
PI ADDRESS:	Department of Computer Science 5143 Cass Ave., Room 431 State Hall Detroit, MI 48202

Objectives (unchanged from original): to model and simulate the chemical dynamics of $O(^3P)$ reaction with hydrocarbon droplets (small clusters), liquids, solids, and self-assembled monolayer (SAM) surfaces.

Status of Effort: This final report describes the initial two phases of the overall project. In the first phase, accurate barriers and energetics were calculated for 7 reactions involved in $O(^3P)$ oxidation of hydrocarbons. This was done by MRCI//CASSCF *ab initio* calculations with cc-pVTZ and cc-pVQZ basis sets and extrapolation to the complete basis set limit. For collisions of high-energy $O(^3P)$ atoms with hydrocarbons, the radical products contain sufficient internal energy to undergo unimolecular decomposition. Tests showed that PMP2//UMP2/cc-pVTZ gives accurate energies and transition state properties for these reactions, and this information was also used to characterize the potential energy surface for hydrocarbon oxidation. In the second phase, the PM3 semiempirical quantum chemistry method, with a UHF wavefunction, was modified and parameterized with specific reaction parameters (SRPs) to fit the *ab initio* barriers, reactions energies, and geometries determined in phase 1. The resulting method, PM3-SRP, gives a good fit to the *ab initio* data. The PM3-SRP method was tested in a trajectory study of the $O(^3P) + C_2H_6 \rightarrow OH + C_2H_5$ reaction dynamics. The results agree with experiment. Complete details of both phases of this project are described in two comprehensive papers.

Tianying Yan, William L. Hase, and Charles Doubleday, "Energetics, transition states, and intrinsic reaction coordinates for reactions associated with $O(^3P)$ processing of hydrocarbon materials," *J. Chem. Phys.* **120**, 9253-9265 (2004).

Tianying Yan, Charles Doubleday, and William L. Hase, "A PM3-SRP + Analytic Function Potential Energy Surface Model for $O(^3P)$ Reactions with Alkanes. Application to $O(^3P)$ + Ethane" *J. Phys. Chem. A*, accepted for publication.

Introduction. Reactions of the electronically ground-state oxygen atom $O(^3P)$ with hydrocarbons are of considerable interest because of their importance in combustion and atmospheric chemistry,[1,2,3] and in processing hydrocarbon surfaces.[4] Extensive gas-phase studies of $O(^3P)$ reaction with alkanes (RH) at low collision energies, where the only reactive channel is

$$O(^3P) + RH \rightarrow OH\cdot + R\cdot$$

have provided detailed information of product internal state distributions,[2,3] scattering angles of the reaction products,[3] and rate constants.[5] For the $O(^3P)$ + CH_4 and $O(^3P)$ + C_2H_6 reactions studied here, the recommended expressions for the thermal rate constants are, respectively, $(1.15 \times 10^{-15}) T^{1.56} \exp(-4270/T)$ $cm^{-3}molecule^{-1}s^{-1}$ for T = 300-2500 K[6] and $(1.8 \times 10^{-31}) T^{6.5} \exp(-140/T)$ $cm^{-3}molecule^{-1}s^{-1}$ for T = 298-1300 K.[7] Some uncertainties remain in the temperature-dependent rate constants as illustrated by the alternative expression $(2.69 \times 10^{-18}) T^{2.3} \exp(-3570/T)$ $cm^{-3}molecule^{-1}s^{-1}$ suggested[8] for $O(^3P)$ + CH_4.

$O(^3P)$ is used in chemical processing of hydrocarbon surfaces to make polymeric materials for technological and industrial applications.[9] Chemical processing by $O(^3P)$ atoms may also be detrimental by damaging polymeric coatings. This is particularly problematic for spacecraft in a low Earth orbit (LEO).[10] Spacecraft in LEO travel at a velocity of approximately 8 km/s, giving rise to a relative translational energy of ~5 eV for an O-atom striking the spacecraft. Under such harsh conditions there is considerable erosion of the spacecraft's surface. Recently, several experimental[4,11,12] and computational studies[13,14,15] have been performed to probe the kinetics and mechanisms for $O(^3P)$ reactions with hydrocarbon surfaces.

At high collision energies other reaction channels, in addition to reaction (1), are open for the $O(^3P)$ atom. From *ab initio* calculations, Massa and coworkers[16] identified a C-C bond

rupture channel, which for ethane forms CH_3 and OCH_3. Schatz and coworkers[14,15] extended these calculations and also identified a C-H bond rupture channel; i.e. $O(^3P) + RH \longrightarrow H + OR$. For the $O(^3P) + C_2H_6$ system the threshold energy is approximately 2 eV for both the C-C and C-H bond rupture channels.[15] For high collision energies, such as 5 eV in LEO, it is expected that a large amount of energy will be deposited in the internal modes of the ethoxy radicals by the C-C and C-H bond rupture channels, leading to unimolecular dissociation of the species. Schatz and coworkers[15,17] have performed direct dynamics simulations with the MSINDO semiempirical theory to study the primary reaction channels for $O(^3P) + C_2H_6$ collisions at 3.26 eV to compare with the experimental study[17] of Minton and coworkers. In this report we describe a similar direct dynamics simulation at 5 eV using a PM3-SRP semiempirical model, in which the trajectories are integrated for a sufficiently long time to investigate the dissociation of the alkoxy radicals formed by the primary reaction channels.

1.1. Multi-reference ab initio calculations.[18] Electronic structure calculations based on multi-configuration wave functions were used to investigate the energetics, transition states, and intrinsic reaction coordinates of a set of prototypical reactions for $O(^3P)$ processing of hydrocarbon molecules and surfaces. The specific reactions studied are

$$O(^3P) + CH_4 \rightarrow OH\cdot + CH_3\cdot \quad (1)$$

$$O(^3P) + C_2H_6 \rightarrow OH\cdot + C_2H_5\cdot \quad (2)$$

$$O(^3P) + C_2H_6 \rightarrow CH_3O\cdot + CH_3\cdot \quad (3)$$

$$OH\cdot + C_2H_6 \rightarrow H_2O + C_2H_5\cdot \quad (4)$$

$OH\cdot + C_2H_5\cdot \rightarrow H_2O +$ 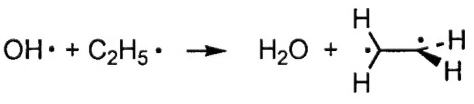 (5)

$$OH\cdot + C_2H_5\cdot \rightarrow H_2O + CH_3\ddot{C}H \quad (6)$$

For all reactions except (4), only the lowest triplet state is examined. Singlet spin states are not considered. Reactions (4) – (6) are possible secondary reactions of the product of reaction (2). Reaction (5) gives triplet ethylene, $^3C_2H_4$, which is twisted 90°. Reaction (6) gives triplet methylcarbene, $^3CH_3CH$.

Reactions (1)-(6) were examined with CASSCF,[19] second and third order Rayleigh-Schrödinger perturbation theory with a CASSCF reference (CASPT2,[20,21] CASPT3[20]), and internally contracted multi-reference configuration interaction (MRCI).[22] The calculations were performed using MOLPRO 2002.3[23] for ROHF, CASSCF, CASPT2/3, and MRCI, and GAMESS 98[24] for the IRC calculations with CASSCF. At CASSCF and CASPT2 optimized geometries, single point energy corrections are computed with MRCI+Q (MRCI with the Davidson correction for quadruple excitations) and the cc-pVTZ and cc-pVQZ basis sets (abbreviated vtz and vqz), with extrapolation to the complete basis set limit (designated CBL) using two-point power law extrapolation.[25] For reactions (1) - (6), the active spaces were (10,10), (8,8), (4,4), (9,9), (10,10), (8,8), respectively. Geometry optimization and frequency calculations were carried out with CASSCF/vtz for all reactions, and also with CASPT2/vtz for reactions (1) - (3).

Table 1 summarizes the CASPT2/CBL and MRCI+Q/CBL 0 K barriers and energies of reaction. The best agreement (within experimental error) is found for MRCI+Q/CBL applied to reaction (1), the only reaction for which the active space preserves the full symmetry of reactants, transition state, and products, while still including all orbitals that undergo significant bonding changes. The MRCI+Q/CBL 0 K energies of reaction for reactions (2) - (6) are more endothermic than experiment by 3-5 kcal/mol. A likely reason for the discrepancies is that, except for reactions (1) and (3), the CASSCF active spaces do not treat the C-H bonds uniformly

for reactants, TS, and products. The small (4,4) active space of reaction (3) contains no C-H bonds and accuracy is not expected. Another source of error in reactions (4) - (6) is that MRCI was not able to accommodate reference spaces that include all the bonds that undergo significant changes during the reactions.

Table 1. CASPT2/CBL and MRCI+Q/CBL values of barriers and energies of reaction at 0 K for reactions (1) - (6).[a]

	Barrier at 0 K			Energy of reaction at 0 K		
	CASPT2	MRCI+Q	best estimate	CASPT2	MRCI+Q	expt[b]
1	7.9	10.5	10 ± 1[c]	-0.1	1.4	1.6 ± 0.2
2	5.3	9.0	7 ± 1[d]	-4.6	-1.4	-5.5 ± 1.4
3	41.3	46.9		2.9	1.1	-1.9 ± 1.0
4	0.6	2.8	1 - 2[e]	-18.8	-17.4	-21.3 ± 1.4
5	1.4	3.2		-19.0	-17.8	-22.7 ± 4
6	2.0	3.8		-10.7	-10.8	-14.4 ± 5

[a]Geometries optimized with CASPT2/vtz for reactions 1 and 2, CASSCF/vtz for others.
[b]http://srdata.nist.gov/cccbdb, IV.A.1 Reaction Comparison. Experimental Enthalpies at 0 K.
[c]O. Roberto-Neto, F. B. C. Machado, and D. G. Truhlar, *J. Chem. Phys.* **111**, 10046 (1999).
[d]Reference 18.
[e]Classical barrier from Y.-Y. Chuang, E. L. Coitino, and D. G. Truhlar, *J. Phys. Chem. A* **104**, 446 (2000); ZPE taken from CASSCF(9,9)/vtz frequencies.

The CASPT2/CBL 0 K energies of reaction do not deviate uniformly from the MRCI+Q/CBL results. CASPT2 is more exothermic than MRCI+Q for reactions (1), (2), (4), and (5), and is within experimental error for reaction (2). CASPT2 is more endothermic than MRCI+Q for reaction (3), and for reaction (6) both methods give essentially the same 0 K energy of reaction. Part of the reason for the irregular deviation from MRCI+Q is mentioned above, that for reactions (4) - (6) the MRCI reference space is a subset of the CASSCF active space but the CASPT2 reference space is the CASSCF active space. In addition, the nonuniform treatment of

C-H bonds in the active spaces of reactants, TS, and products for reactions (2) - (6) may affect CASPT2 and MRCI differently.

Comparison of the MRCI+Q/CBL energetics for reactions (1), (2), and (4) suggests that the accuracy of MRCI+Q/CBL is limited mainly by the quality of the active space, which properly describes reactants, TS, and products for reaction (1) but is biased for reactions (2) and (4). Barriers computed with CASPT2/CBL are consistently lower than those computed with MRCI+Q/CBL. Comparison with the three best estimates sugggests that CASPT2 underestimates all six barriers, at least with the current active spaces. A systematic way to improve the results would be to increase the size of the active space with a series of RASSCF reference spaces.[26]

For reactions (1) and (2), geometry optimization is carried out with both CASSCF and CASPT2. The position of the abstracted H atom between the C and O atoms in the TS is significantly closer to C with CASPT2 than with CASSCF. However, this change in TS geometry does not appreciably change the CASPT2/CBL or MRCI+Q/CBL barriers.

Published calculations of reactions (1) - (4) with a single-reference wave function and a basis set of vtz quality or better give generally good results, but none involve basis set extrapolation. Without basis set extrapolation, apparent agreement with experiment is accidental in the sense that improvement in the basis set could lead to worse agreement. In most of the calculations previously applied to reactions (1) - (4), vtz is the highest level basis set employed. Therefore, it is useful to know how much the barriers and energies of reaction change from the vtz level to the CBL level. Since extrapolation of CASPT2 and MRCI+Q changes the energetics by similar amounts, average energy changes are summarized here. Barriers of reactions (1) – (6) computed with CBL are lower than those computed with vtz by 2.1, 1.7, 2.4, 1.2, 1.1, and 0.5

kcal/mol, respectively. Energies of reaction computed with vtz become more negative at the CBL level by 3.2, 3.4, 2.8, 2.7, 2.6, and 1.9 kcal/mol. The effect is greater for reaction energies than for barriers, and is also greater for the $O(^3P)$ reactions (1) – (3) than for the reactions of OH. Barriers of the triplet disproportionations, reactions (5) and especially (6), are the least sensitive.

1.2. Single reference ab initio calculations. The abstraction reaction forming OH is the only primary reaction of $O(^3P)$ + alkanes at low collision energies. Among the secondary reactions, only those involving OH are important for this energy regime. However, at higher energies C-H and C-C bond ruptures become important primary reactions, and secondary bimolecular and unimolecular reactions involving their radical products may occur. Figure 1 shows barrier heights and heats of reaction for the three primary reaction channels and for secondary reactions involving the products of these channels. The energies not in parentheses are PMP2/vtz//UMP2/vtz values calculated as part of this project. The energies in parentheses for channels P1, P3, S1, and S2 in Figure 1 are the MRCI/CBL values in Table 1. PMP2/vtz is close to MRCI/CBL for these cases, a presumably fortuitous result because the latter is extrapolated. This notwithstanding, in the PM3-SRP fitting described in the next section, PMP2/vtz was substituted for MRCI/CBL when the latter was not available.

For high energy collisions between $O(^3P)$ and hydrocarbons, the products of the primary reactions may contain sufficient energy to undergo unimolecular dissociation reactions. Figure 2 shows unimolecular dissociations UD*n* for the products of the $O(^3P)$ + C_2H_6 primary and secondary reactions in Figure 1.

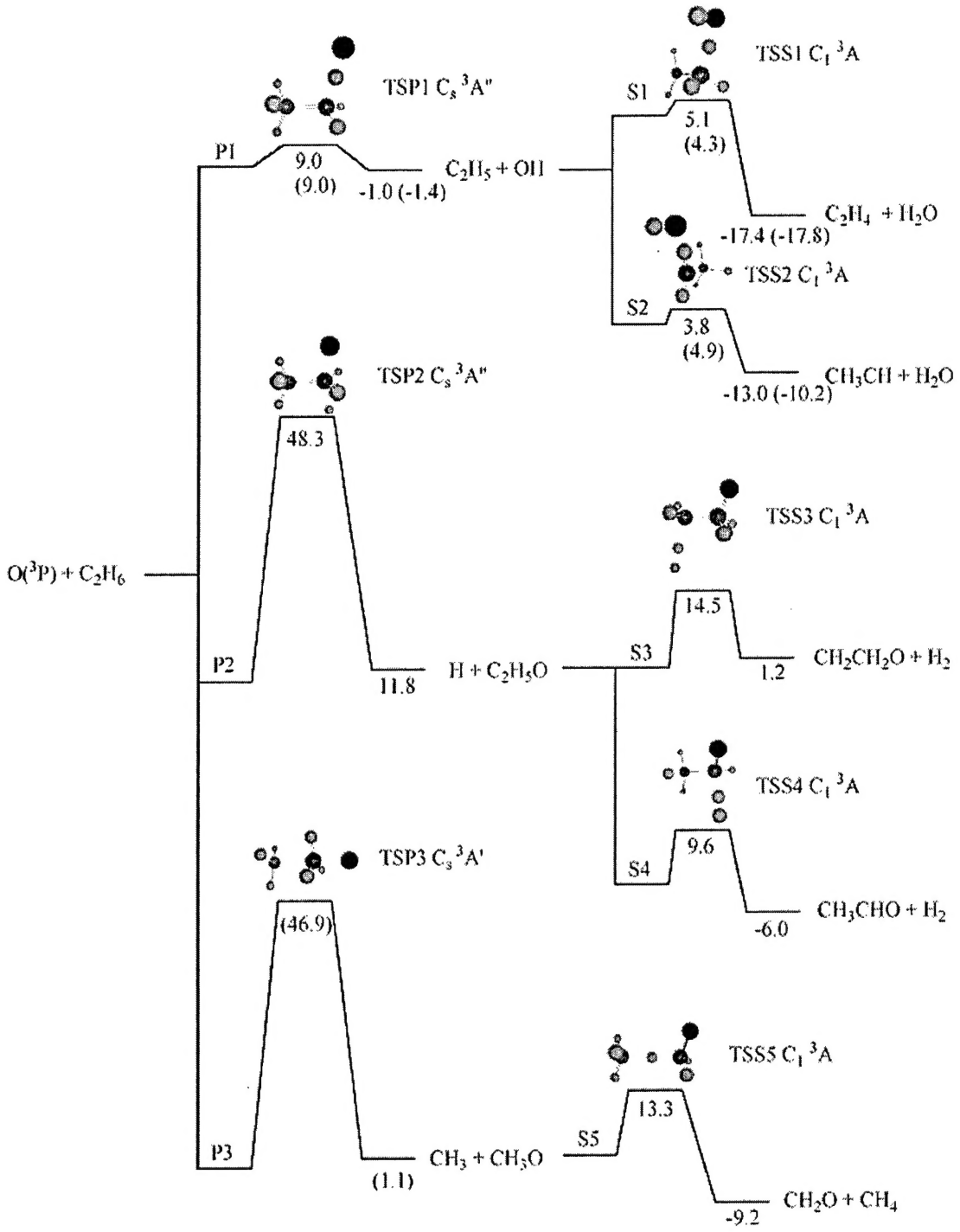

Figure 1. Barrier heights and 0 K heats of reaction for the primary reactions of $O(^3P)$ + ethane (P1-P3) and secondary reactions involving products of the primary reactions. Energies not in parentheses were calculated PMP2/vtz//UMP2/vtz. Energies in parentheses are the MRCI values from Table I.

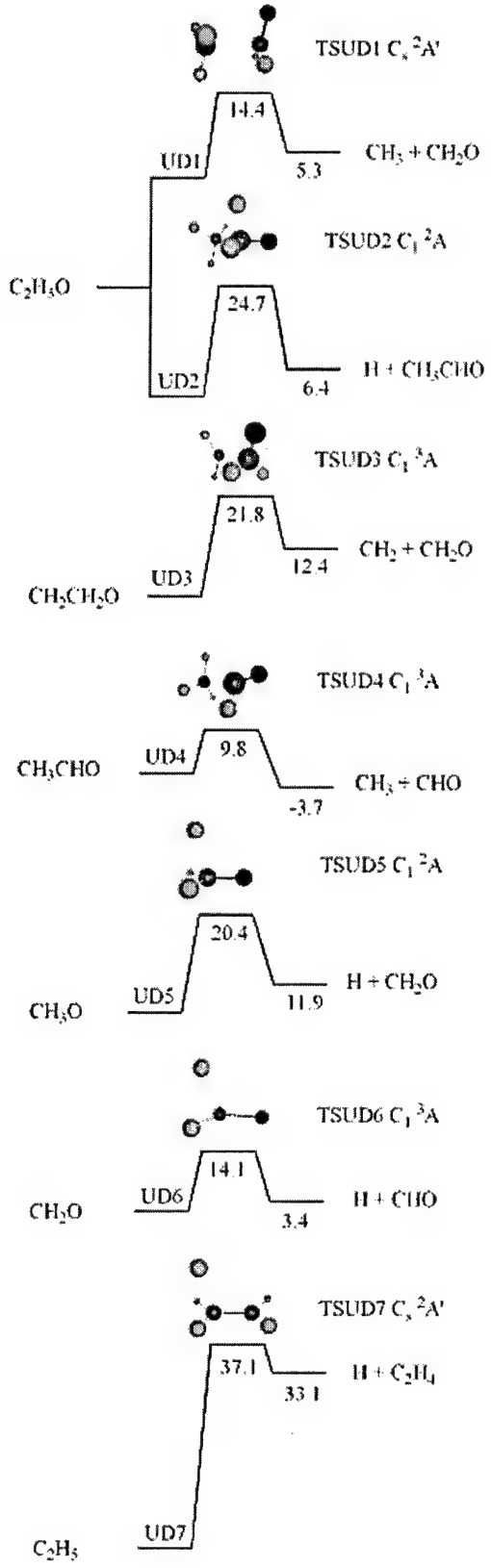

Figure 2. Barrier heights and 0 K heats of reaction for unimolecular dissociations of some of the products of reactions in Figure 1, calculated with PMP2/vtz//UMP2/vtz.

2. Development and parametrization of PM3-SRP potential. As the basis of the QM potential, we chose the PM3 method in the Mopac 7 package,[27] using the triplet UHF wavefunction with analytical derivatives. To construct the PM3-SRP hamiltonian, we modified the form of certain integrals as described below, then reparametrized PM3-SRP to fit the ab initio barriers, reaction energies, and geometries.

The PM3-SRP Hamiltonian is constructed with 65 parameters. 29 of these are conventional PM3 parameters for C, O, H (12, 12, and 5 parameters) accessible through the 'external' keyword in Mopac. The remaining 36 parameters are associated with modified resonance integrals given by

$$H_{ij}^{ab} = \chi_{ij}^{ab}(R_{ij}) H_{ij}^{0,ab},$$

where $\chi_{ij}^{ab}(R_{ij})$ is a distance-dependent scaling factor[28,29] and $H_{ij}^{0,ab}$ is the PM3 resonance integral between atoms i and j, ab labels the overlap type (ss, sp, pp), and R_{ij} is the i-j distance. The scaling factor is defined by

$$\chi_{ij}^{ab}(R_{ij}) = \chi_{ij,R_{small}}^{ab} + \frac{1}{2}\left(\chi_{ij,R_{large}}^{ab} - \chi_{ij,R_{small}}^{ab}\right)\left[1 + \tanh\left(f_{ij}\left(R_{ij} - R_{ij}^{0}\right)\right)\right],$$

which switches from $\chi_{ij,R_{small}}^{ab}$ at small values of R_{ij} to $\chi_{ij,R_{large}}^{ab}$ at large distance. R_{ij}^{0} is the distance at which the switch is turned on half way, and f_{ij} governs the rate at which the switch operates.

$$V = V_{PM3\text{-}SRP} + V_{analytic}$$

$$V_{analytic} = \frac{1}{2}\sum_{O-C,O-H}\left[a\exp(-br) + c/r^{6}\right]\left[1 + \tanh\left(\alpha\left(r - r_{0}\right)\right)\right]$$

To include van der Waals interactions, the total potential V used for trajectories is where r is the O-C or O-H distance. The tanh function turns off $V_{analytic}$ at short distance.

The fitting involves minimizing the sum of squares

$$w_E^2 \sum_i \left(E_i - E_i^0\right)^2 + w_R^2 \sum_i \left(R_i - R_i^0\right)^2 + w_A^2 \sum_i \left(A_i - A_i^0\right)^2 + w_D^2 \sum_i \left(D_i - D_i^0\right)^2$$

where the difference terms involve PM3-SRP minus ab initio energies, bond lengths, bond angles, and dihedral angles, and *w* are weighting factors. The *Fortran GA* genetic algorithms program of D. A. Carroll was used.[30]

Two PM3-SRP models, Models 1 and 2, were developed for $O(^3P) + C_2H_6$ by fitting structures and energies of reactant, transition state, and product stationary points for two groups of reactions. For Model 1 the MRCI energies and structures of the stationary points for reactions (1) – (6) were fit. These reactions are relevant to low energy O + alkane collisions. In Model 2, appropriate for high energy collisions, the PMP2/vtz energies and structures for 14 reactions were included in the fit; i.e. all reactions in Figures 1 and 2 except reaction UD7 in Figure 2. The fitting for Model 2 also included the long-range potential $V_{analytic}$ for $O(^3P) + CH_4$. Model 2 was developed after trajectory simulations of $O(^3P) + C_2H_6$ collisions showed the participation of many different reactions.

A comparison between PM3-SRP Model 1 and MRCI/CBL is given in Table 2. The fit was based on the first six reactions. Overall, there is good agreement. PM3-SRP Model 2 and *ab initio* energetics are compared in Table 3. The requirement to fit a larger number of reactions for Model 2 decreases the accuracy of the barrier for reactions P2, S3, and S4 relative to Model 1. In addition, the barriers for UD2 - UD5 are inaccurate, as are the heats of reaction for UD4 and UD6. This may be associated in part with the use of a simple UHF wavefunction with minimal basis set.

Table 2. MRCI, PM3, and PM3-SRP Energetics of Primary and Secondary Reactions[a,b]

Reaction[c]	MRCI		PM3		PM3-SRP Model 1		PM3-SRP Model 2	
	$\Delta E^{\ddagger}$	ΔE^{0}	$\Delta E^{\ddagger}$	ΔE^{0}	$\Delta E^{\ddagger}$	ΔE^{0}	$\Delta E^{\ddagger}$	ΔE^{0}
$O(^3P) + CH_4 \rightarrow OH + CH_3$	10.5	1.4	7.0	-19.9	10.5	3.9	8.8	-8.7
$O(^3P) + C_2H_6 \rightarrow OH + C_2H_5$	9.0	-1.4	4.2	-27.8	7.0	-7.9	10.7	-16.0
$OH + C_2H_6 \rightarrow C_2H_5 + H_2O$	2.8	-18.0	5.4	-25.3	3.9	-14.3	7.6	-18.6
$OH + C_2H_5 \rightarrow H_2O + {}^3C_2H_4$	4.3	-17.8	7.0	-22.5	5.8	-12.8	8.9	-17.3
$OH + C_2H_5 \rightarrow H_2O + {}^3CH_3CH$	4.9	-10.2	5.1	-17.7	2.6	-9.5	7.9	-10.4
$O(^3P) + CH_3\text{-}CH_3 \rightarrow CH_3O + CH_3$	46.9	1.1	25.9	-29.1	47.2	3.0	51.3	-5.7
$O(^3P) + CH_3\text{-}CH_3 \rightarrow C_2H_5O + H$[d]	48.3	11.8	24.4	-5.9	32.1	19.1	34.5	9.2

[a]Energies are in kcal/mol and include zero point vibrational energy corrections. Ab initio frequencies were computed by CASSCF/vtz as described for Table 1.
[b]See Table 1 for experimental 0 K heat of reaction.
[c]Ground state triplet potential energy surface.
[d]PMP2/vtz//UMP2/vtz energies; not included in the PM3-SRP fitting for Model 1.

Table 3. PM3-SRP Model 2 *vs ab initio* energies (kcal/mol).[a]

Reaction	PM3-SRP Model 2		*ab initio*	
	$\Delta E^{\ddagger}$	ΔE^{0}	$\Delta E^{\ddagger}$	ΔE^{0}
P1[b]	9.0	-16.0	9.0	-1.4
P2	34.5	9.2	48.3	11.8
P3	51.3	-5.7	46.9	1.1
S1	8.9	-17.3	4.3	-17.8
S2	7.9	-10.4	4.9	-10.2
S3	0.1	-3.7	14.5	1.2
S4	-1.5	-8.3	9.6	-6.0
S5	6.8	-12.0	13.3	-9.2
UD1	16.5	0.1	14.4	5.3
UD2	9.1	14.2	24.7	6.4
UD3	15.1	11.3	21.8	12.4
UD4	22.3	6.5	9.8	-3.7
UD5	8.5	15.0	20.4	11.9
UD6	14.2	20.6	14.1	3.4

[a]ZPE corrected (0 K energies).
[b]P1, P3, S1, and S2 are calculated with MRCI+Q/CBL, all others with PMP2/vtz//UMP2/vtz.

3. $O(^3P) + C_2H_6$ reaction dynamics. Trajectory calculations were performed to study the dynamics of reactions at a collision energy of 5 eV. The PM3-SRP potential energy function was used for these calculations.

3.1.1. Computer program and trajectory initial conditions. The direct dynamics simulation was carried out by interfacing the general chemical dynamics package VENUS[31] with the semiempirical electronic structure package MOPAC 7,[27] with the necessary modifications to include the distance-dependence scaling factors[28,29] and the long range potential $V_{analytic}$. The resulting package is called VENUS-MOPAC.[32] Quasiclassical normal mode sampling[33,34] was used to sample a canonical ensemble of C_2H_6 molecules for the trajectories. The vibrational energy for each normal mode was sampled according to a 300 K Boltzmann distribution, and, together with the ZPE, added to the normal mode with a random vibrational phase. The system so prepared, in normal mode coordinates, is transformed to Cartesian coordinates. A rotational energy is added to each rotational degree of freedom according to a 300 K classical Boltzmann distribution. The initial separation between $O(^3P)$ and the C_2H_6 center-of-mass is set to be 6 Å, with C_2H_6 randomly orientated. The impact parameter b is sampled from $b = b_{max}\xi^{1/2}$, where ξ is chosen uniformly on $0 \leq \xi \leq 1$ and $b_{max} = 3.5$ Å, which is large enough to encompass all reactive events. With this procedure, the impact region is sampled uniformly within a circle of 3.5 Å radius. The initial $O(^3P)$ and C_2H_6 relative translational energy is fixed at 5 eV. The c.m. velocity of the whole system $[O(^3P) + C_2H_6]$ is 0 and the system represents a c.m. frame, not a lab. frame. The above procedures are standard options in VENUS.[31] A total of 50000 and 50107 trajectories were calculated for Models 1 and 2, respectively, to have a detailed description of the complex $O(^3P) + C_2H_6$ reaction dynamics.

3.1.2. Integrating the classical equations of motion. To calculate the classical trajectories, Hamilton's equations of motion are integrated by VENUS[31] with a combined 4th-order Runge-Kutta and 6th-order Adams-Moulton predictor-corrector algorithm.[35] PM3-SRP is incorporated into MOPAC and is called whenever potential energy and/or its derivatives are needed. There are two criteria for terminating a trajectory: (1) non-reactive trajectories are terminated when the center-of-mass separation between $O(^3P)$ and C_2H_6 is larger than 7 Å after the collision's inner turning point in the $O(^3P)$ and C_2H_6 relative motion; (2) reactive trajectories are integrated up to 500 fs to monitor possible secondary reactions including the unimolecular dissociations in Figures 1 and 2.

To calculate the potential energy and its derivatives for the PM3-SRP model, the SCF convergence criterion is set to 10^{-4} kcal/mol for fast convergence. For each trajectory, a fresh guess of the density matrix is used for the first integration step, and the converged density matrix is then used for a good initial guess for the following integration steps. The integration time step is reduced to 0.1 fs for this fast collision (5 eV) system and, with this small time step, relatively few SCF iterations are needed to converge the density matrix. There are some trajectories that experience one or two convergence failures during the integration as $O(^3P)$ approaches C_2H_6, particularly near a transition state structure.[28] When SCF failure occurs, a fresh guess of the density matrix is generated and a more sophisticated Camp-King converger,[36] one of MOPAC 7 convergence options, is used and this usually results in a converged density matrix, though it is slow. However, about 0.4% of the trajectories still experience SCF convergence failure after this second try and therefore are discarded. Another 0.2% of the trajectories do converge, but converge to a state different than the desired triplet, and are also discarded. Energy is conserved to within 1 kcal/mol for the trajectories retained.

3.2. Trajectory Results. The $O(^3P)$ + C_2H_6 reaction dynamics determined from the trajectory calculations for PM3-SRP Models 1 and 2 are presented in the following. The calculations were performed for a relative translational energy of 5 eV and C_2H_6 rotational/translational temperature of 300 K.

3.2.1. Opacity functions. Opacity functions, probability of reaction versus impact parameter *b*, for both Model 1 and 2 are shown in Figure 3 for several product channels. Overall

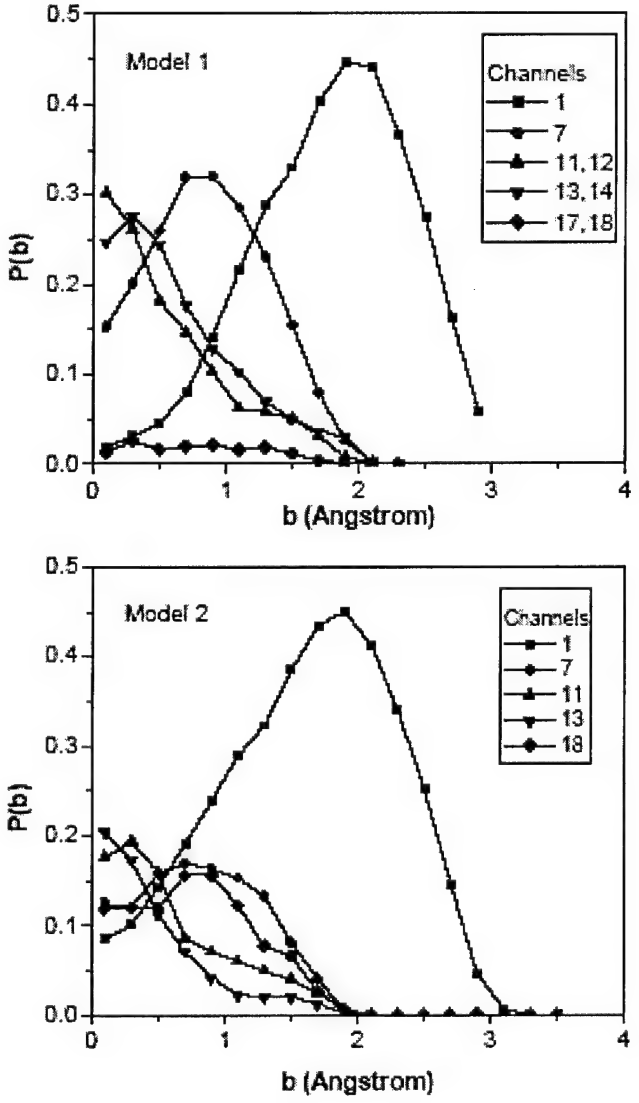

Figure 3. Opacity functions for five of the product channels calculated with Models 1 and 2.

there is very good agreement between the opacity functions for the two models. For Model 1, opacity functions are given which combine channels 11 and 13 and channels 12 and 14. However, since channels 11 and 13 dominate these opacity functions, they may be compared with the Model 2 opacity functions for channels 11 and 13. The only substantial difference in the results for the two models is for channel 18, whose reaction probability is much larger for Model 2. Both models show that the reaction probabilities for channels 11 and 13 increase as the impact parameter approaches zero. For channels 1, 7, and 8 the opacity function peaks at intermediate parameters, with the peak at ~ 2 Å for channel 1 and at smaller values of *b* for the other two channels. Similar opacity functions, for multiple product channels, is a marker that they may occur by the same type of reaction dynamics. The peaking in the opacity function for channel 1, OH formation, at a large value of *b* suggests it occurs by a "stripping" mechanism. This is the only important reaction that occurs at impact parameters larger than 2.1 Å. There are no reactive trajectories at an impact parameter larger than about 3.2 Å.

The opacity function for channel 1, as a function of the vibrational state of the OH product, is given in Figure 4. There is a tendency for the opacity function to flatten and broaden, and its peak move to a larger *b* as the vibrational level increases. The relative population of the 0, 1, and 2 vibrational states is 1 : 0.80 : 0.38.

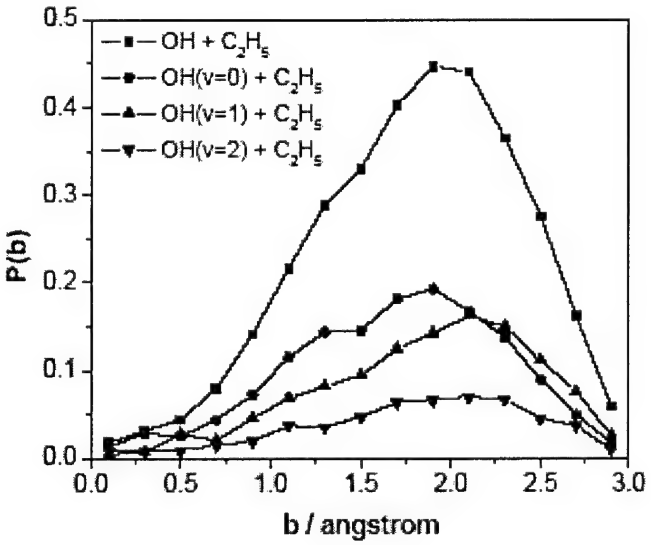

Figure 4. Opacity function for channel 1 as a function of the OH vibrational state. Calculations are for Model 1.

3.2.2. Reactive cross sections. Cross sections for the different product channel are listed in Table 4. Statistical uncertainties are not included, since with more than 50000 trajectories for

Table 4. Reaction cross sections of different channels.

Channel	Products[a]	Apparent reaction path[b]	Cross section, Å^2	
			Model 1	Model 2
1	$OH + C_2H_5$	P1	7.14	7.76
2	$C_2H_5O + H$	P2	0.30	0.009
3	$CH_3O + CH_3$	P3	0.025	0.014
4	$OH + C_2H_4 + H$	P1 → UD7	0.082	0.046
5	$H_2O + {}^3C_2H_4$	P1 → S1	0.031	0.019
6	$H_2O + CH_3CH$	P1 → S2	0.31	0.14
7	$CH_3CHO + 2H$	P2 → UD2	2.06	1.17
8	Ethylene oxide + 2H	P2 → UD2 → isom[c]	0.13	0.057
9	$CH_2CH_2O + H_2$	P2 → S3	0.021	< 0.001
10	$^3CH_3CHO + H_2$	P2 → S4	0.087	< 0.001
11	$CH_2O + CH_3 + H$	P2 → UD1 P3 → UD5	0.80	0.65
12	$CH_2O + CH_2 + H_2$	P2 → S3 → UD3	0.026	0.042
13	$CHO + CH_3 + H_2$	P2 → S4 → UD4	0.77	0.41
14	$CHO + CH_4 + H$	P3 → S5 → UD6	0.27	0.071
15	$CH_2CHO + H_2 + H$			0.20
16	$CH_2{=}C{=}O + H_2 + 2H$		0.060	0.072
17	$C_2H_2O + 2H_2$		0.17	0.007
18	$CO + CH_3 + H_2 + H$		0.14	0.93
19	$CO + CH_2 + 2H_2$			0.084
20	$CO + CH_4 + 2H$			0.016
21	$CH_3CHOH + H$	P2 → isom		0.061
22	$^3CH_2{=}CHOH + H_2$	P2 → S3 → isom		0.014

[a]Ground state triplet potential energy surface.
[b]Nomenclature for reaction paths is defined in Figures 1 and 2.
[c]Isom means the product isomerizes.

each model the uncertainties are quite small. A substantial amount of the 5 eV high collision energy is deposited into the methoxy, CH_3O, and ethoxy, C_2H_5O, products of channels 3 and 2

and, as a result, these primary products undergo secondary unimolecular reactions. This leads to a large number of reaction products and small cross sections for channels 2 and 3. Since channel 1 occurs by a stripping mechanism as suggested by Figure 3, only a small fraction of the 5 eV collision energy is deposited in the C_2H_5 product. Little dissociation of C_2H_5 to H + C_2H_4 occurs, as shown by the large cross section for channel 1 and the much smaller cross section for channel 4. Because of the importance of unimolecular dissociation for the products of primary channels 2 and 3, the cross sections calculated from the trajectories strongly depends on the length of time the trajectories are integrated. Fewer product channels would have been observed if the trajectories were only integrated for 100 ps instead of the 500 ps calculated here. Indeed, the trajectory cross sections may change and additional products formed if the trajectories were integrated for an even longer time. Some of the products observed at 500 ps may have sufficient energy to unimolecularly dissociate on a longer timescale.

There are important relationships between the many product channels presented in Table 4. For channels 5 and 6, as the OH radical departs it abstracts another H-atom. The resulting H_2O formation is dynamically controlled, since the two abstracted H-atoms tend to come from the same methyl group; i.e. the cross section for channel 6 is an order of magnitude larger than that for channel 5. This result was also observed by Schatz and co-workers.[15] The CH_3O methoxy radical of channel 3 can dissociate to H and H_2CO, forming channel 11, and possibly also to H_2 + HCO, forming channel 13. The energies for this latter channel were not investigated in our *ab initio* calculations.[37] If HCO retains sufficient internal energy, it will dissociate to H + CO, yielding channel 18. The CH_3 and CH_3O products of channel 3 may undergo a secondary reaction, forming CH_4 and triplet CH_2O, which will dissociate to H + HCO, yielding channel 14.

If HCO then dissociates to H + CO, the products of channel 20 are formed. Thus, channels 11, 13, 18, 14, and 20 may originate from primary channel 3.

Quite a large number of reactions are promoted by primary channel 2. The vibrationally excited C_2H_5O radical product may dissociate either a H-atom or CH_3 radical, forming acetaldehyde and formaldehyde, respectively, for channels 7 and 11. For channel 8 acetaldehyde is in its cyclic ethylene oxide (i.e. oxirane) isomeric structure. The ethoxy radical has isomerized to its enol structure in channel 21. Though the total heat of reaction for each of these two channels is highly endothermic (63.7 kcal/mol and 51.5 kcal/mol with PM3-SRP Model 2), the 5 eV collision supplies sufficient energy as long as it is efficiently transferred to internal energy of the ethoxy radical.

The H-atom product from channel 2 may undergo a secondary reaction, abstracting an H-atom to form H_2 and the triplet species in channels 9, 10, and 22. For channels 9 and 10 the two H-atoms forming H_2 come from different and the same carbon atoms, respectively, while the triplet enol in channel 22 is an isomer of those in channels 9 and 10. Because of the low barriers for unimolecular decomposition of these triplet species, the cross sections for their formation are small. The relative importance of channels 9 and 10 may be established from the cross sections for products which originate from these two channels. The triplet biradical in channel 9 dissociates to CH_2O and $^3CH_2$ to give the products in channel 12. Triplet acetaldehyde in channel 10 dissociates to either the CH_3 + HCO products in channel 13 or to H and CH_3CO, with the latter possibly dissociating to give the CH_3 + CO products in channel 18. Similarly, the HCO product of channel 13 may dissociate to H + CO forming the channel 18 products. Thus, both channels 13 and 18 may follow channel 10. Regardless of the importance of channel 18 in this sequence, that the cross section for channel 13 is an order of magnitude larger than that for

channel 12 shows that channel 10 is much more important than channel 9. The dominance of channel 10 shows that the two H-atoms eliminated from C_2H_5O to form H_2 tend to come from the same carbon atom in a manner similar to how H_2O is formed.

The above discussion shows that channels 7, 8, 9, 10, 11, 12, 13, 18, 21, and 22 may originate from primary channel 2. Given the channels associated with primary channels 1 and 3, the only channels that have not been related to a primary channel are channels 15, 16, 17, and 19. Channel 15 may follow channel 20, when the CH_2CHOH triplet radical dissociates to CH_2CHO + H. Channel 16 may be an additional step in this sequence, with CH_2CHO dissociating to CH_2CO (ketene) + H. Possible precursors for channel 17, and formation of triplet ketene, is the elimination of H_2 from the triplet radical products in channels 9, 10, and 22. One possible pathway for channel 19 is dissociation of triplet ketene in channel 17. It should be recognized that these are only conjectures concerning the sequence of reactions leading to product channels 15, 16, 17, and 19. However, given the nature of the products for these channels, it seems likely that they are initiated by primary channel 2.

To compare Models 1 and 2 and to compare the relative importance of primary channels 1, 2, and 3 (P1, P2, and P3), it is useful to sum the cross sections for the product channels associated with each primary channel. Some of the product channels are associated with both P2 and P3 and one-half of the cross sections for these channels is contributed to both P2 and P3. The product channels 1 and 4 - 6 are associated with P1, channels 2, 7 – 10, 11(1/2), 12, 13(1/2), 15 - 17, 18(1/2), 19, 21, and 22 are associated with P2, and channels 3, 11(1/2), 13(1/2), 14, 18(1/2), and 20 associated with P3. Using this analysis, the Model 1 primary cross section for P1, P2, and P3, before any ensuing events, are estimated as 7.56, 3.71, and 1.15 $Å^2$, and for Model 2 as 7.97, 2.65, and 1.10 $Å^2$. These sets of cross sections are in good agreement. Channel 1 is the most

important primary channel, consistent with the previous simulation of this system by Schatz and co-workers.[15] In comparing the Model 1 and Model 2 cross sections in Table 4 for the different product channels, one sees that decomposition of the ethoxy product of channel 2 is less important for Model 1 than for Model 2, giving rise to a much larger cross section for this channel with Model 1. Also, the cross section for channel 18, which follows channel 13, is much larger for Model 2. It is worth noting that the sum of the cross sections for channels 13 and 18 is 0.91 and 1.34 $Å^2$, respectively, for Models 1 and 2 and not that different. Overall, Models 1 and 2 give similar patterns in the cross sections for the different product channels.

In concluding this section, we need to point out a shortcoming of the PM3-SRP parameters. As shown in Table 3, Model 2 predicts essentially no barriers for the secondary reactions S3 and S4, while the *ab initio* barriers are 10 – 15 kcal/mol. As a result, H_2 formation via these channels is expected to be artificially high. Channel 18 is significant for Model 2, and a route to this channel is through channel 10, which occurs by the P2 → S4 step. The triplet aldehyde in channel 10 may decompose to give CH_3 + H + CO sequentially or nearly simultaneously. The result is that Model 2 predicts a significant amount of CO, which may be too large as a result of a too high probability of H_2 formation. Thus, the validity of the proposed CO formation needs to be examined by experiment. However, for 5 eV collision of $O(^3P)$ with C_2H_6, CO is a likely product. In a recent experimental study of the $O(^3P)$ + C_2H_5 reaction, by time-resolved Fourier transform infrared emission spectroscopy, CO was observed as a product.[38] The trajectories calculated here predict the formation of formaldehyde, by decomposition of the ethoxy radical in path P2 to CH_3 + H_2CO or decomposition of the methoxy radical in path P3 to H + H_2CO. The former was previously proposed by Vivier-Bunge and co-workers.[39]

3.2.3. Angular distributions. Product scattering angles within the c.m. frame are often measured for A + B → C + D reactions.[40] A crossed-beam experiment usually measures just one of the products, and the other is completely determined since the c.m. motion remains constant. A lab. to c.m. transformation[41] is then applied to determine the scattering angles in the c.m. frame. For the direct dynamics simulation carried out here, there are up to three or four fragments for some of the channels, i.e. the prototype reactions A + B → C + D + E and A + B → C + D + E + F. Though the scattering angle can be calculated from the trajectory without ambiguity, an additional assumption is necessary to measure the scattering angle experimentally. Since the channels with three or four products involve H-atom(s) and/or H_2 molecule(s), a valid assumption is that, because they are light, they do not significantly affect the motion of the heavier products. This kinematics is illustrated in Figure 5 for a prototype reaction A + B → C + D + H (or H_2), where the center-of-mass (c.m.') of the products C + D may be approximated to

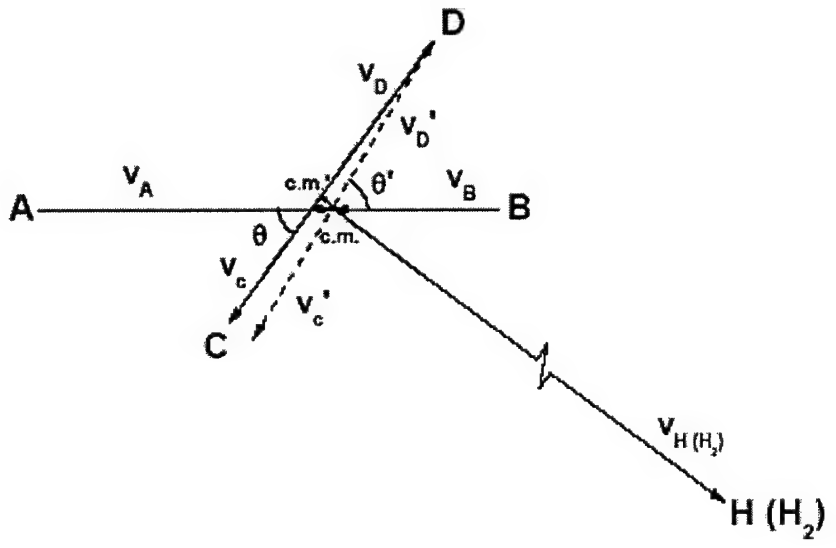

Figure 5. Velocity vector diagram of A + B → C + D + H (or H_2) prototype reaction in the c.m. frame. If H (or H_2) is much lighter than C and D, the real deflection angle θ can be well-represented by angle θ' (A + B → C + D prototype reaction) by neglecting H (or H_2).

reside on the center-of-mass (c.m.) of the whole system. By such an approximation, the reaction is reduced to the conventional A + B → C + D reaction. The deflection angle θ' for the above approximation can be measured experimentally. The real deflection angle is denoted as θ in Figure 5. With a computer simulation, one can calculate both θ and θ' to examine the accuracy of this approximation. Because the products of the primary channels P2 and P3 may undergo significant secondary and unimolecular dissociation reactions, the experimental scattering angles for these channels do not reveal the nascent scattering dynamics, before the secondary and dissociation reactions. Thus, probing the scattering dynamics of the non-primary channels is of considerable importance and it is necessary to test the above approximate approach for determining their scattering angles.

Figure 6 shows the normalized differential cross sections (NDCS) of several channels with OH, CH_2O, CHO and CO as products, determined from the Model 2 trajectories. Though acetaldehyde is found to be the second most important product in this study, its NDCS is not calculated since it will primarily move with the c.m. motion by eliminating two light H-atoms and a crossed-beam experimental measurement in the laboratory frame would detect most of them at the c.m. scattering angle. This makes it difficult to draw a dynamical picture for this channel. For the same reason, the NDCS of channel 2, with C_2H_5O as a product, is not calculated. Also there are very few trajectories for this channel, since most of the C_2H_5O radicals decompose as discussed above. The NDCS of channel 3, with CH_3O as product, is also not calculated since its reaction cross section is very small, with only 18 trajectories forming this product.

The NDCS for channels 1 and 4, with OH as a product, is shown in Figure 6. There is almost no ambiguity in the scattering angle for this channel using the conventional prototype A +

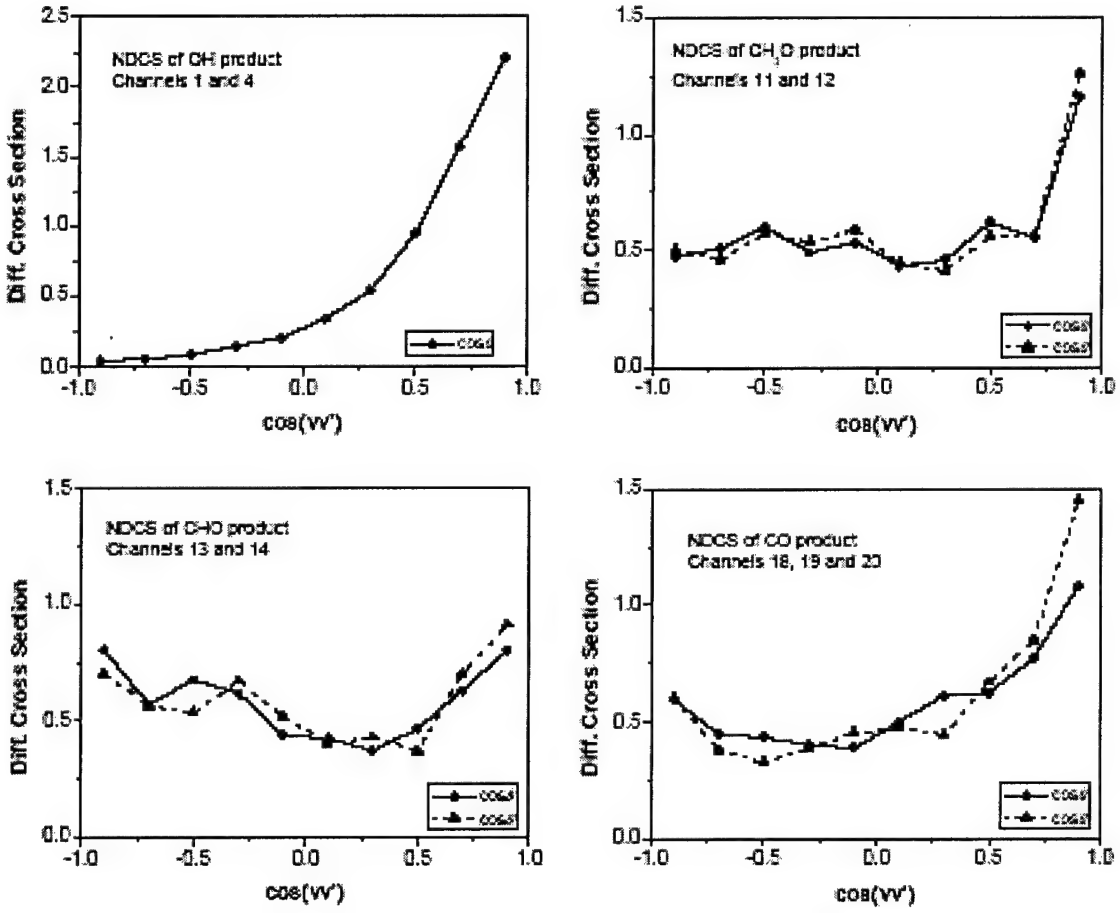

Figure 6. The normalized differential cross sections, $(1/\sigma)(\Delta\sigma/\Delta(\cos\theta))$, for different channels (see Table 4). $\Delta(\cos\theta) = 0.2$ for the curves. Results are based on Model 2.

$B \rightarrow C + D$ reaction, because channel 4 contributes an insignificant amount of OH. The angular distribution of OH is mostly forward scattered, the same as Schatz and co-workers[14] found. The forward scattering is consistent with a stripping mechanism. Channel 4 is mainly associated with small impact parameters which primarily fall in the range of 0.6 – 1.2 Å. These collisions, which have a small probability, deposit sufficient energy in the C_2H_5 product of P1 that it can dissociate to $H + C_2H_4$.

The angular distribution for the CH_2O product of channel 11 and 12 is shown in Figure 6. The scattering angles θ and θ' are defined in Figure 5. The NDCS of the actual scattering is plotted by the solid line, and the scattering angle determined by ignoring the light H-atom is

plotted by the dashed line. The similarity of the two curves illustrate the validity of the assumption of neglecting the light product. There are several important features in this angular distribution: (1) the strong forward scattering indicates a mechanism, in which $O(^3P)$ abstracts one of the methyl groups from C_2H_6 to form a forward scattered CH_3O analogous to H-abstraction, as previously discussed by Schatz and co-workers.[14] The energetic CH_3O radical then eliminates an H-atom to form formaldehyde and; (2) the flat region with a $\cos\theta$ value less than 0.6 and a minimum in the scattering probability near 90° are indicative of a long-lived collision complex.

Figure 6 shows the NDCS for channels 13 and 14, with the HCO radical as the product. The curve for the actual scattering is given by the solid line and the curve from ignoring the H_2 molecule or H-atom is given by the dashed line. For these two channels, the NDCS is quite symmetric, indicating a long-lived collision complex prior to formation of HCO. Also given in Figure 6 is the NDCS for CO, a product of channels 18, 19, and 20. These channels are 4-product systems (see Table 4) with double H-atom(s) and/or H_2 molecule(s) eliminations. As a consequence, the difference between the actual scattering angle θ and the approximate scattering angle θ' is large in comparison to the difference for the other plots in Figure 6. Except for the forward scattering component in the distribution, the NDCS for CO is more symmetric than are the NDCS's for the other products in Figure 6, suggesting that CO may be formed through a longer-lived intermediate (or intermediates) as compared to those for the other products. The forward scattering asymmetry suggests some of the CO products are formed directly or through a very short-lived collision complex.

3.3. Comparison with previous cross-beam experiments and direct dynamics simulations.

Minton and co-workers[17] have studied the $O(^3P) + C_2H_6$ reaction in crossed-beams at a collision energy of 3.5 eV. They identified the primary channels P1, P2, and P3, leading to OH + C_2H_5, C_2H_5O + H, and $CH_3O + CH_3$ in their experiments. The same primary channels are observed in our simulations. However, they did not observe the large number of additional product channels, arising from secondary and unimolecular dissociation reactions of the primary channels' products, as found in our simulations. These secondary and unimolecular reactions become more important as the collision energy is increased, and that our simulation is performed at energy 1.5 eV higher than that for the experiments is expected to be an important factor in understanding differences between the experiments and our simulations. It is also possible that higher resolution in the experimental measurements may reveal more products.

Minton and co-workers[42] investigated the decomposition of the OCH_3 radical in a crossed-beam study of the $O(^3P) + CH_4 \rightarrow H + OCH_3$ reaction at a collision energy of 2.9 eV. Since the reaction endothermicity is 0.62 eV, the energy available to the reaction products is 2.3 eV = 52.6 kcal/mol. MSINDO direct dynamics simulations of this reaction by Troyà et al.[15] give 0.40 as the fraction of the available energy partitioned to OCH_3 internal energy. Thus, for this experiment, the internal energy of the OCH_3 product is estimated as 21 kcal/mol and lower than the 33 kcal/mol estimated (see below) for this product in the simulations reported here of $O(^3P) + C_2H_6 \rightarrow CH_3 + OCH_3$. Minton and co-workers concluded that a significant fraction of their OCH_3 product dissociates to $H + H_2CO$ and a small fraction isomerizes to CH_2OH, with a relative H_2CO:OCH_3:CH_2OH product yield of 0.73 : 0.22 : 0.05. Minton and co-workers observation of less OCH_3 decomposition and fewer decomposition products, as compared to the results of the simulations reported here, is consistent with the lower OCH_3 internal energy in their experiments.

Troya et al. performed[15] a semiempirical MSINDO direct dynamics simulation to study the $O(^3P) + C_2H_6$ reaction at collision energies ranging from 0.65 to 5.75 eV. Their calculations at 3.92 and 5.75 eV bracket the simulations reported here for 5 eV and may be interpolated to compare with the current results. In comparison to our trajectories, which were integrated for 500 fs, Troya et al.[15] integrate their trajectories for a much shorter period of time.[43] They observed the primary channels $OH + C_2H_5$, $C_2H_5O + H$, and $CH_3O + CH_3$ with interpolated cross sections at 5 eV of 5.32, 3.53, and 1.06 $Å^2$, respectively. The cross sections from our simulations are in overall good agreement with these values. The Model 1 and 2 cross sections for channel 1 are 7.56 and 7.97 $Å^2$ and somewhat larger than the MSINDO cross section. This difference with MSINDO is similar to the difference observed between PM3 and MSINDO for the $O(^3P) + CH_4 \rightarrow OH + CH_3$ cross section,[15] which suggests that the PM3-SRP models retain the characteristic of giving a cross section larger than MSINDO for $O(^3P) + RH \rightarrow OH + R$ abstraction. Models 1 and 2 cross sections for channel 3, of 1.15 and 1.10 $Å^2$, are in excellent agreement with the Troya et al. value of 1.06 $Å^2$. During the short time of Troya et al.'s trajectory simulations three additional product channels were observed; i.e. channels 5 – 7 forming $H_2O + C_2H_4$, $H_2O + CH_3CH$, and $CH_3CHO + 2H$. The cross section for channel 6 is much larger than that for channel 5, which is the same as found from Models 1 and 2. The cross section interpolated to 5 eV for channels 5 + 6 and channel 7 are 0.56 and 0.056 $Å^2$, respectively. Troya et al.'s cross section for channel 7 is substantially smaller than the values of 2.06 and 1.17 $Å^2$ for Models 1 and 2, but their value is expected to increase if their trajectories were integrated for a longer period of time, allowing more dissociation of C_2H_5O.

Energy partitioning to reaction products, other than OH, was not determined in our simulations. However, Troya et al. analyzed the product energy partitioning for the primary

product channels and their results at 3.92 and 5.75 eV may be used to estimate the energy partitioning at 5 eV. For the OH + C_2H_5 products the average partitioning is estimated to be 0.74 to translation, 0.16 to C_2H_5 internal, and 0.10 to OH rotation and vibration. For the H + C_2H_5O products the energy partitioning is estimated as 0.36 to translation and 0.64 to C_2H_5O internal energy. For the CH_3O + CH_3 products the estimated energy partitioning is 0.71 to translation, 0.29 to CH_3O internal and 0.00 to CH_3 internal energy. Deposition of large amounts of energy into the C_2H_5O and CH_3O radical products is consistent with the extensive dissociation we observe for these products. The average internal energy available to the C_2H_5O product is the 5 eV collision energy minus the 11.8 kcal/mol reaction endothermicity for channel 2 (see Figure 1) multiplied by the 0.64 average fraction partitioned to C_2H_5O, which equals 66 kcal/mol. As shown in Figure 2, this average energy is in large excess of that required for C_2H_5O unimolecular dissociation. The 33 kcal/mol average internal energy of the CH_3O product is also in excess of that required for dissociation. The energy partitioning to the C_2H_5O and CH_3O products of the primary channels indicates they will undergo extensive unimolecular decomposition as seen in our simulations.

Finally, the rotational and vibrational energy distributions found by Troya et al. for the OH product of channel 1 are similar to the results of our simulations, which are shown in Figure 7. They performed their analyses for a collision energy of 0.65 eV and found that the rotational distribution peaked at j = 15. We find at a collision energy of 5 eV that the peak is slightly dependent on the OH vibrational state v and is at j = 18, 15, 14 for v = 0, 1, 2, respectively. The relative population of the OH v=0 : v=1 : v=2 states is 1 : 0.80 : 0.38. Troya et al's relative population is 1 : 0.53 : 0.063, which has more v=0 and less v=2 than our results. This is consistent with their lower collision energy.

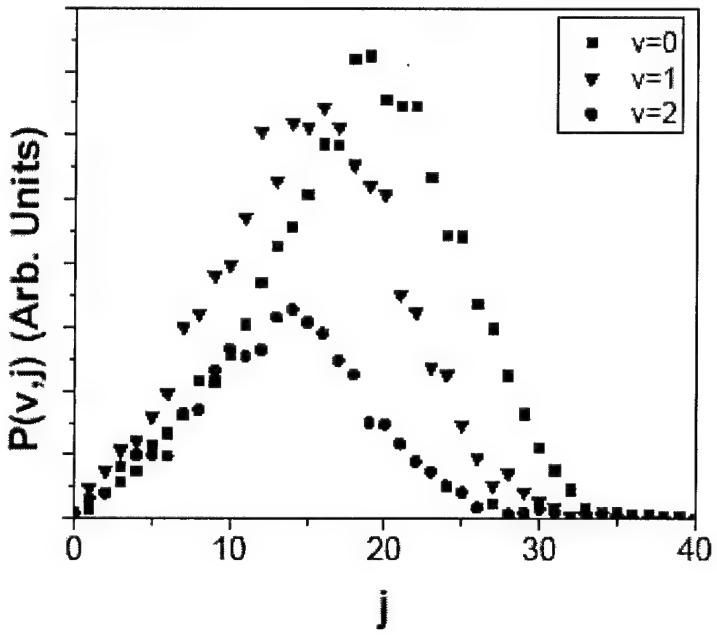

Figure 7. Vibrational and rotational energy distributions for the OH products of channel 1.

References

1 P. Andresen and A. C. Luntz, J. Chem. Phys. **72**, 5842 (1980).

2 F. Ausfelder and K. G. McKendrick, Prog. Reac. Kinet. Mech. **25**, 299 (2000).

3 H. Tsurumaki, Y. Fujimura, and O. Kajimoto, J. Chem. Phys. **112**, 2000 (2000).

4 D. J. Garton, T. K. Minton, M. Alagia, N. Balucani, P. Casavecchia, and G. G. Volpi, Faraday Discuss. Chem. Soc. **108**, 387 (1997); J. Zhang, D. J. Garton, and T. K. Minton, J. Chem. Phys. **117**, 6239 (2002).

5 A. Migoshi, K. Tsuchiya, N. Yamauchi, and H. Matsui, J. Phys. Chem. **98**, 11452 (1994).

6 D. L. Baulch, C. J. Cobos, R. A. Cox, C. Esser, P. Frank, T. Just, J. A. Kerr, M. J. Pilling, J. Troe, R. W. Walker, and J. Warnatz, J. Phys. Chem. Ref. Data **21**, 411 (1992).

7 N. Cohen and K. R. Westberg, J. Phys. Chem. Ref. Data **20**, 1211 (1991).

8 J. C. Corchado, J. Espinosa-Garcia, O. Roberto-Neto, Y.-Y. Chuang, and D. G. Truhlar, J. Phys. Chem. A **102**, 4899 (1998).

9 T. P. Nguyen, A. Lahmar, and P. Jonnard, J. Adhesion **66**, 303 (1998); M. S. Hartney, D. W. Hess, and D. S. Soane, J. Vac. Sci. Technol. **B7**, 1 (1989); O. Joubert, J. Pelletier, and Y. Arnal, J. Appl. Phys. **65**, 5096 (1989); C. M. Chan, T. M. Ko, and H. Hiraoka, Surf. Sci. Rep. **24**, 1 (1996).

10 T. K. Minton and D. J. Garton, in *Chemical Dynamics in Extreme Environments*, edited by R. A. Dressler (World Scientific, Singapore, 2001), pp. 420; E. Grossman and I. Gouzman, Nucl. Instruments Methods Phys. Res. B **208**, 48 (2003).
11 D. J. Garton, T. K. Minton, M. Alagia, K. Balucani, P. Casavecchia, and G. G. Volpi, J. Chem. Phys. **112**, 5975 (2000).
12 T. K. Minton, J. Zhang, D. J. Garton, and J. W. Seale, High Performance Polymers **12**, 1 (2000); H. Kelso, S. P. K. Kohjer, D. A. Henderson, and K. G. McKendrick, presented at the the 19th Conference on the Dynamics of Molecular Collisions, 2003 (unpublished).
13 G. Li, S. B. M. Bosio, and W. L. Hase, J. Mol. Struct. **556**, 43 (2000).
14 D. Troya, R. Z. Pascual, and G. C. Schatz, *J. Phys. Chem. A*, **107**, 10497 (2003).
15 D. Troya, R. Z. Pascual, D. J. Garton, T. K. Minton, and G. C. Schatz, J. Phys. Chem. A **107**, 7161 (2003).
16 A. Gindulyte, L. Massa, B. A. Bands, and S. K. Rutledge, J. Phys. Chem. A **104**, 9976 (2000).
17 D. J. Garton, T. K. Minton, D. Troya, R. Pascual, and G. C. Schatz, J. Phys. Chem. A **107**, 4583 (2003).
18 T. Yan, W. L. Hase, and C. Doubleday, *J. Chem. Phys.* **120**, 9253-9265 (2004).
19 H.-J. Werner and P. J. Knowles, J. Chem. Phys. **82**, 5053 (1985); P. J. Knowles and H.-J. Werner, Chem. Phys. Lett. **115**, 259 (1985).
20 H.-J. Werner, Mol. Phys. **89**, 645 (1996).
21 P. Celani and H.-J. Werner, J. Chem. Phys. **112**, 5546 (2000).
22 H.-J. Werner and P. J. Knowles, J. Chem. Phys. **89**, 5803 (1988); P. J. Knowles and H.-J. Werner, Chem. Phys. Lett. **145**, 514 (1988).
23 MOLPRO, a package of ab initio programs designed by H. -J. Werner and P. J. Knowles, version 2002.3 (2002). R. D. Amos, A. Bernhardsson, A. Berning, P. Celani, D. L. Cooper, M. J. O. Deegan, A. J. Dobbyn, F. Eckert, C. Hampel, G. Hetzer, P. J. Knowles, T. Korona, R. Lindh, A. W. Lloyd, S. J. McNicholas, F. R. Manby, W. Meyer, M. E. Mura, A. Nicklab P. Palmieri, R. Pitzer, G. Rauhut, M. Schütz, U. Schumann, H. Stoll, A. J. Stone, R. Tarroni, T. Thorsteinsson, and H.-J. Werner.
24 M. W. Schmidt, K. K. Baldridge, J. A. Boatz, S. T. Elbert, M. S. Gordon, J. H. Jensen, S. Koseki, N. Matsunaga, K. A. Nguyen, S. Su, T. L. Windus, M. Dupuis, and J. J. A. Montgomery, J. Comput. Chem. 14, 1347 (1993).
25 A. Halkier, T. Helgaker, P. Jorgensen, W. Klopper, H. Koch, J. Olsen, and A. K. Wilson, Chem. Phys. Lett. 286, 243 (1998).
26 P. Celani and H.-J. Werner, J. Chem. Phys. **112**, 5546 (2000).
27 J. J. P. Stewart In *Reviews in Computational Chemistry*; Lipkowitz, K. B., Boyd, D. B., Eds.; Wiley: New York, 1990.
28 Doubleday, C.; Nendel, M.; Houk, K. N.; Thweatt, D.; Page, M. *J. Am. Chem. Soc* **1999**, *121*, 4720.
29 Doubleday, C. *J. Phys. Chem. A* **2001**, *105*, 6333.
30 Carroll, D. A. *http://cuaerospace.com/carroll/ga.html*.
31 Hase, W. L.; Duchovic, R. J.; Hu, X.; Kormonicki, A.; Lim, K.; Lu, D.-H.; Peslherbe, G. H.; Swamy, K. N.; Linds, S. R. V.; Varandos, A. J. C.; Wang, H.; Wolf, R. J. *QCPE* **1996**, *16*, 671.

32 Peslherbe, G. H.; Bolton, K.; Doubleday, C.; Hase, W. L. VENUS-MOPAC, a General Chemical Dynamics and Semiempirical Direct Dynamics Compoter Program, To be released.
33 Chapman, S.; Bunker, D. L. *J. Chem. Phys.* **1975**, *62*, 2890.
34 Hase, W. L.; Ludlow, D. M.; Wolf, R. J.; Schlick, T. *J. Phys. Chem.* **1981**, *85*, 958.
35 Press, W. H.; Teukolsky, S. A.; Vetterling, W. T.; Flannery, B. P. *Numerical Recipes in Fortran*; Cambridge University Press, 1992.
36 Camp, R. N.; King, H. F. *J. Chem. Phys.* **1981**, *75*, 268.
37 Barriers and heats of reaction were not calculated for the CH_3O -> H_2 + HCO and C_2H_5O -> CH_4 + HCO unimolecular decompositions. Using the experimental 0 K enthalpies from the NIST database (http://srdata.nist.gov/cccbdb), the 0 K heats of reaction for the former reaction is 5.0 kcal/mol. The PMP2/vtz//UMP2/vtz calculations give -1.5 and -12.4 kcal/mol for these 0 K heats of reaction. The reaction C_2H_5O -> H_2 + CH_3CO, also expected to be nearly thermoneutral, was not studied by the PMP2 calculations.
38 Reid, J. P.; Marcy, T. P.; Kuehn, S.; Leone, S. R. *J. Chem. Phys.* **2000**, *113*, 4572.
39 Alvarez-Idaboy, J. R.; Diaz-Acosta, I.; Vivier-Bunge, A. *J. Comput. Chem.* **1997**, *19*, 811.
40 Levine, R. D.; Bernstein, R. B. *Chemical Reaction Dynamics and Chemical Reactivity*; Oxford: New York, 1987.
41 Lee, Y. T. In *Atomic and Molecular Beam Methods*; Scoles, G., Ed.; Oxford: New York, 1988; Vol. 1.
42 Troya, D.; Schatz, G. C.; Garton, D. J.; Brunsvold, A. L.; Minton, T. K. *J. Chem. Phys.* **2004**, *120*, 731.
43 Troya et al, ref.15, stopped their trajectories when two products were seperated by 6.3 A. For H-atom elimination or abstraction the integration time is less than 50 fs. For elimination of the heavier CH_3 radical, the integration time is expected to be less than 100 fs.

Personnel Supported: Dr. Charles Doubleday, Department of Chemistry, Columbia University, Tianying Yan, a Ph.D. graduate student at Wayne State University, and Samip Mehra a M.S. graduate student at Wayne State University. Tianying completed his Ph.D. degree the end of August 2003 and joined the Greg Voth research group at the University of Utah as a post-doctoral associate.

Publications:

Tianying Yan, William L. Hase, and Charles Doubleday, "Energetics, transition states, and intrinsic reaction coordinates for reactions associated with $O(^3P)$ processing of hydrocarbon materials," *J. Chem. Phys.* **120**, 9253-9265 (2004).

Tianying Yan, Charles Doubleday, and William L. Hase, "A PM3-SRP + Analytic Function Potential Energy Surface Model for $O(^3P)$ Reactions with Alkanes. Application to $O(^3P)$ + Ethane" *J. Phys. Chem. A*, accepted for publication.

Interactions/Transitions:

a. **Meetings** – This work was presented at the AFOSR Molecular Dynamics/Theoretical Chemistry Contractors Meeting held May 18 – 21, 2003 in San Diego, CA; at the 19th Conference on the Dynamics of Molecular Collisions held July 13 – 18, 2003 at Lake Tahoe, CA; at the Annual Review of the AFOSR/MURI project "Materials Degradation/Passivation in the Space Environment" held August 19 – 20, 2003 at the University of Pittsburgh; and in a seminar given to the Department of Chemistry, Virginia Tech University on August 29, 2003.

b. **Consultative and Advisory Functions:** None.

c. **Transitions:** None to date, but expected for the future.

New Discoveries, Inventions, or Patent Disclosures: None.

Honors/Awards:

Participant in the NRC Workshop on *Challenges for the Chemical Sciences in the 21st Century: Workshop on Information and Communications,* Board on Chemical Sciences and Technology, The National Academies, Washington, D.C., October 31 – November 2, 2002; Chaired the morning session, November 2.
Vice-Chair, 7th Winter Gordon Conference on *Gaseous Ions: Structure, Energetics and Reactions,* March 2 – 7, 2003, Ventura, CA.

Fellow in the American Physical Society, 1991

Elected to Lifetime Membership in the Academy of Scholars of Wayne State University, 1994

Fellow in the American Association for the Advancement of Science, 1997

Distinguished Professor of Chemistry, Wayne State University, 1997